SIAM J. Applied Dynamical Systems
Vol. 10, No. 4, pp. 1502–1524

Continuity of Resetting a Pacemaker in an Excitable Medium*

Bartłomiej Borek†, Leon Glass†, and Bart E. Oldeman†

Abstract. Pacemakers in excitable media generate waves that propagate outward from the pacemaker. Such waves of excitation are well known in biological and chemical systems such as nerves, the heart, and the Belousov–Zhabotinsky reaction. Stimuli delivered at a distant site from the pacemaker can reset the pacemaker, leading to a change in the timing of the pacemaker. The relation between stimulus timing and resultant resetting of the pacemaker is captured by phase resetting curves. The continuity of resetting curves has been investigated in both experiments and numerical models. We present theoretical results discussing conditions for continuity of resetting curves as the amplitude and phase of the stimulus varies. We also use continuation and shooting methods to analyze the continuity of resetting curves in simple mathematical models of cardiac and neural activity. Under continuous changes of stimulus parameters, resetting curves will be continuous unless a stimulus leads to dynamics that fall outside the basin of attraction of the pacemaker-driven excitable medium.

Key words. phase resetting, excitable systems, pacemaker, basin of attraction, continuation method, traveling wave

AMS subject classifications. 37N25, 37C10, 35K57, 35Q92, 65P99

DOI. 10.1137/100819229

1. Introduction.

Biological oscillations are essential to life and underlie key physiological functions from the beating of the heart to reproductive cycles. In order to understand the interactions of oscillations with the environment and with each other, experimentalists have determined the effects of single or repeated perturbation on oscillations. Concurrently, there has been theoretical analysis of the fundamental properties of biological oscillations and their response to perturbation. A geometric perspective was developed by Winfree, who considered the response of a limit-cycle oscillation in ordinary differential equations to stimuli delivered at various phases of the oscillation [39, 40]. Winfree posed several conjectures related to phase resetting that were subsequently examined from a topological perspective by Guckenheimer [16].

Winfree defines a phase transition curve that gives the phase of an oscillation subsequent to a perturbation delivered at a phase φ (for formal definitions see section 2). Provided that the state point following the perturbation remains in the basin of attraction of the limit cycle for a stimulus delivered at any phase of the cycle, the phase transition curve must be a continuous function that maps the unit circle onto itself. This *Continuity Theorem* is true for oscillations in ordinary differential equations [16] and partial differential equations [12].

*Received by the editors October 21, 2010; accepted for publication (in revised form) by J. Guckenheimer October 3, 2011; published electronically December 13, 2011. This work was partially supported financially by NSERC, MITACS, and the Canadian Heart and Stroke Foundation.
http://www.siam.org/journals/siads/10-4/81922.html
†Department of Physiology, Centre for Applied Mathematics in Bioscience and Medicine, McGill University, 3655 Promenade William Osler, Montréal QC, H3G 1Y6, Canada (borek@cnd.mcgill.ca, glass@cnd.mcgill.ca, boldeman@cnd.mcgill.ca).

Although examination of the Continuity Theorem has not been a focus of experimental studies, apparent discontinuities have been observed [40, 18]. There are at least two potentially different theoretical mechanisms that may lead to discontinuities in phase transition curves [15]: (i) Phase transition curves can be continuous but very steep in appropriate theoretical models formulated as differential equations; (ii) for some phase, or range of phases, a perturbation may displace the state point outside of the basin of attraction of the limit cycle, so that the continuity theorem no longer holds.

Krogh-Madsen et al. found an example of an apparent discontinuity, in a numerical study of resetting in an ionic model of cardiac cells [26]. By using continuation methods with AUTO [9] for stimulus phase and amplitude parameters close to those for which there is a sharp change in the phase transition curve, they show that all perturbed trajectories stay in the basin of attraction of the limit cycle so that the resetting curve is steep but not discontinuous. In a real biological system, the phase transition curve would be so steep that to resolve the continuity might demand voltage resolutions smaller than the voltage changes induced by the opening or closing of a single channel. This could provide a mechanism for experimental observations of discontinuous phase resetting [18].

A numerical study of resetting a circulating pulse in a one-dimensional ring provided an example in which the system was shifted outside its basin of attraction by appropriately timed stimuli [13]. In this example, carrying out resetting with a single stimulus at low temporal resolution gives rise to discontinuous phase transition curves. However, by probing the phases finely near the discontinuous resetting in a range of phases called the vulnerable period [38], stimuli were identified which led to a single retrograde wave. When this retrograde wave collided with the anterograde wave, both waves were annihilated, thereby shifting the dynamics outside of the basin of attraction of the original dynamics. However, additional studies of resetting in a related model, in which re-entry occurs on a one-dimensional ring with a tail, showed discontinuous resetting even though there was no evidence for stimuli which would lead to annihilation of the re-entry [36, 14, 25]. Similarly, numerical results on the resetting of a pacemaker embedded in a two-dimensional excitable medium appeared to lead to discontinuous resetting curves [19], even though no stimuli led to dynamics lying outside the basin of attraction of the pacemaker. These findings are in apparent contradiction to the theory. In the following we show that examination of continuity of resetting curves using shooting methods may be inadequate due to very steep changes in resetting behavior as a function of stimulus parameters.

Continuation provides an alternative to shooting to investigate resetting curves [26, 6, 29]. Continuation methods are particularly suitable for investigating resetting in continuous ordinary or partial differential equations in settings where there are strong divergences between trajectories arising from neighboring initial conditions. In the current context, we change either the phase or the amplitude of a stimulus and apply continuation methods in two different fashions originally utilized to compute manifolds [24]. (i) *Fixed integration time*: we carry out integration for a fixed length of time as the initial condition varies. By continuity of the differential equations, the endpoint of the integration and the trajectories will change continuously as the initial condition varies [16]. (ii) *Constrained endpoint*: we carry out the integration using a boundary condition criterion in which we track the trajectories until the state point returns to the vicinity of a point on the stable limit cycle attractor. In this case,

if, as a parameter changes, some initial conditions are not in the basin of attraction of the limit cycle attractor, then continuation methods will fail.

Phase transition curves were first directly computed through continuation by using a fixed integration time of $3T_0$, where T_0 is the period of the cycle, in [6]. Our approach extends this method so that it can be applied to discontinuous perturbations and partial differential equations and uses a constrained endpoint where desirable.

In the following, we show that the use of continuation methods enables us to find complex dynamics, including one-dimensional spiral waves [23, 11, 7] over tiny ranges of parameter space. The presence of such behaviors may depend sensitively on parameters of the underlying equations as well as the discretization of the domain. Although dynamics occurring over such small regions of parameter space would normally not be considered important for the understanding of real physical or biological systems, the strong analogy between these dynamics and echo waves observed experimentally in biological preparations of Purkinje fiber from mammalian heart [1, 3] suggest a possible implication of these behaviors in situations of reduced cardiac conductivity such as might occur as a result of heart disease.

The plan of the paper is as follows. In section 2 we introduce essential definitions and terminology for the resetting of limit cycle oscillations. As these topics have been discussed at length elsewhere [16, 19, 28, 12, 14], we provide key ideas, and readers should consult the references for more detailed discussions. In section 3 we apply continuation methods to study resetting of an equation in which the Van der Pol oscillator has been modified so that there are three equilibria: a saddle point and two unstable nodes. This illustrates the way the continuation methods can be used to identify initial conditions that lie outside the basin of attraction of the limit cycle oscillation. In section 4, we extend these methods to a case of a pacemaker embedded in a one-dimensional excitable medium modeled by a modified FitzHugh–Nagumo equation. Since cardiac tissue is composed of discrete cells, it is not necessarily appropriate to think of cardiac tissue as a continuous medium [21, 22], and we consider different discretizations of the medium. We show that, depending on the discretization, continuation [9] can reveal very different transient dynamics following a stimulus at a critical phase of the cycle. In particular, we show the presence of one-dimensional spiral waves for coarse discretizations similar to those described recently in the Morris–Lecar equations [7]. Since the one-dimensional spiral provides a mechanism through which discontinuous phase transition curves are possible, in section 5 we use continuation for the Morris–Lecar equations in modified equations with a localized pacemaker. This analysis allows us to confirm and extend the earlier results [7] and also to identify a new type of dynamics in which a pacemaker is entrained to a one-dimensional spiral wave. We conclude with a brief discussion of the results.

2. Mathematical background.

The following technical material is needed for establishing continuity properties of phase resetting following perturbation. The basic formulation is adopted from earlier papers [16, 19, 28, 12, 14], but we present a new result, the Continuity Lemma, which asserts continuity of resetting curves over a range of different types of perturbation.

Assume a dynamical system with a stable limit cycle Γ with period T_0. The limit cycle is assumed to be a hyperbolic attractor. We specify a marker event on the limit cycle which we define as phase 0. For example, for excitable tissue the marker event is usually taken at

the onset of the excitation. As time progresses the state point traces a trajectory $X(t) \in \Gamma$ in state space. If the marker event occurs at time $t = t_0$, then in the absence of perturbations we define the phase of the oscillation as $\varphi(t) = (t - t_0)/T_0 \pmod 1$. Each point on the trajectory $X(t) \in \Gamma$ is also identified by the phase $\varphi(X(t)) = (t - t_0)/T_0 \pmod 1$. Consequently all points on Γ can be identified with a phase.

The *basin of attraction* of Γ, designated $B(\Gamma)$, corresponds to all states that approach Γ in the limit $t \to \infty$. $B(\Gamma)$ is foliated by hypersurfaces called isochrons. In the asymptotic limit $t \to \infty$, all states on an isochron asymptotically approach the same state. Consequently, each isochron is identified by the phase defining the unique state in Γ lying on the isochron.

To help fix ideas, consider a two-dimensional ordinary differential equation with a single unstable steady state and stable limit cycle that is globally attracting for all points except the steady state. The isochrons are curve segments that cut transversely across the limit cycle. All isochrons approach the neighborhood of the steady state as shown in Figure 1. A point $P \in B(\Gamma)$, $P \notin \Gamma$, has the *latent phase* $\varphi_l(P)$ defined as the phase of the isochron containing P. If $P \in \Gamma$, then $\varphi_l(P) = \varphi(P)$. For partial differential equations, all definitions extend naturally, but a point P on an isochron represents a function defining the values of all variables at all points in space.

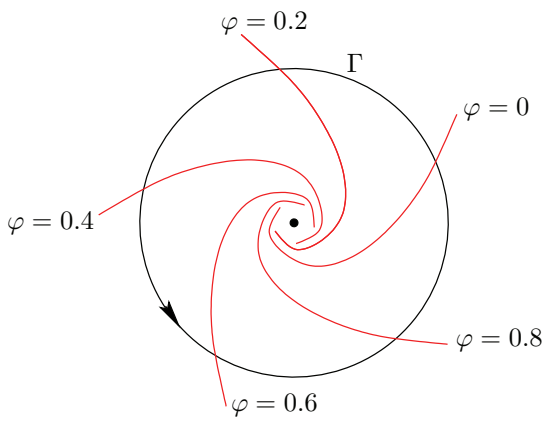

Figure 1. *The isochrons are the red line segments that transversally intersect the attracting limit cycle* Γ *for different phases* φ*. In this schematic figure the velocity along the limit cycle is assumed to be uniform, so the phases are uniformly distributed.*

We now consider a state $X_0 \in B(\Gamma)$ and a continuous perturbation, $\Psi(\mu)$, depending on a variable μ. In traditional studies of phase resetting, $X_0 + \Psi(\mu)$ represents the locus of states in phase space generated by delivering a perturbation for all points on (at all phases of) the cycle. However, $X_0 + \Psi(\mu)$ could equally be generated by other perturbations including changing the amplitude and the location of the stimulus. As long as the stimulation parameters are changed continuously, the following Continuity Lemma holds.

Lemma 2.1 (Continuity Lemma). *If* $X_0 + \Psi(\mu) \in B(\Gamma)$ *for all* μ*, then* $\varphi_l(X_0 + \Psi(\mu))$ *is continuous.*

Although the Continuity Lemma seems obvious, we are not aware of any previous statement of this result. It follows from the continuous dependence of solution curves in differential

equations on initial conditions [17] and the continuity of the phases of isochrons [16, 12].

In the particular case where $X_0+\Psi(\mu)$ is generated by delivering a stimulus to a limit cycle oscillation at all phases of the oscillation, we have the *Continuity Theorem*, and $\varphi_l(X_0+\Psi(\mu))$ is a continuous map of the circle into itself [16, 12]. $\varphi_l(X_0+\Psi(\mu))$ is often called the phase transition curve. In this case, the states defined by $X_0+\Psi(\mu)$ for all μ define the image of the original limit cycle Γ following a perturbation delivered at all phases of the cycle. This is often called the *shifted cycle*. In the current context, if we perturb a limit cycle oscillation by delivering stimuli of varying amplitudes (rather than of varying phases), then we need the Continuity Lemma in order to assert continuity of the phase transition curve delivered as a function of amplitude and provided the stimulus does not lead to a transition outside of the basin of attraction of the limit cycle.

3. Computing the phase transition curve using continuation in an ordinary differential equation. As a first example, we consider a system of ordinary differential equations based on the Van der Pol oscillator, which has been modified so that the single unstable equilibrium is replaced by a saddle and two unstable foci:

$$\begin{aligned} \dot{x} &= \frac{1}{\varepsilon}(-y - x^3 + a^2 x), \\ \dot{y} &= \varepsilon(bx - y), \end{aligned} \tag{3.1}$$

where $a = \sqrt{2}$, $b = 0.1$, and $\varepsilon = 0.1$.

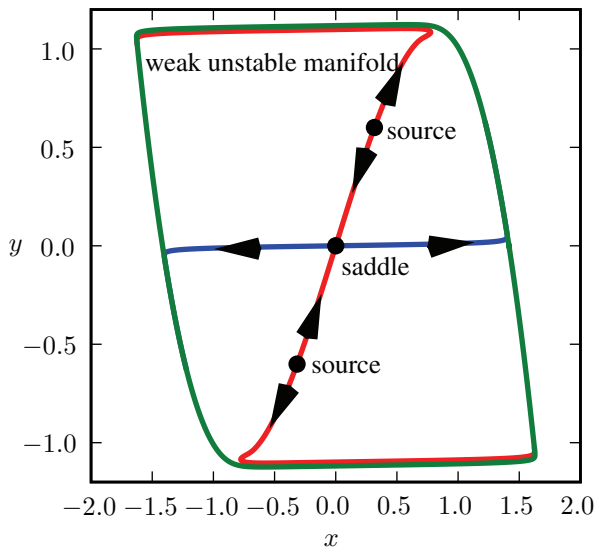

Figure 2. *Phase space for (3.1) with $a = \sqrt{2}$, $b = 0.1$, and $\varepsilon = 0.1$. There are two unstable nodes, a saddle point, and a stable limit cycle oscillation.*

The phase space for this system can be seen in Figure 2. Most initial conditions in this system give rise to orbits that very quickly converge to a stable limit cycle. However, if the shifted cycle crosses the stable manifold of the saddle point, then there is a point on the shifted

cycle that lies outside of the basin of attraction of the limit cycle, and the phase transition curve will be discontinuous. Further, in some cases the shifted cycle can cross the canard trajectory which is formed by the weak unstable manifold, that is, a trajectory tangent to the weak unstable eigenvector of a source. In this case, the shifted cycle will lie entirely in the basin of attraction of the limit cycle, but points near the canard trajectory will take a long time to approach the limit cycle. We illustrate this computation using both continuation methods—*fixed integration time* and *constrained endpoint*. For each of these methods we consider both the situation in which the shifted cycle lies entirely in the basin of attraction of the limit cycle and the situation in which the shifted cycle intersects the stable manifold of the saddle point.

We use standard boundary value problem continuation and bifurcation software in AUTO [9] to continue orbit segments as they depend on parameters. AUTO uses Gauss–Legendre collocation; the orbits are continued as they depend on parameters "as a whole" instead of using numerical integration. This approach is robust against sensitive dependence on initial conditions and was described in [24] and directly applied to compute phase transition curves with a continuous perturbation in [6]. A similar technique has recently been used to compute isochrons for the FitzHugh–Nagumo equation [29].

To obtain the phase transition curve involving a discrete perturbation numerically using continuation techniques, the trajectory is split into two parts, one part $(x_\Gamma(t), y_\Gamma(t))$, $t \in [0, \varphi T_0]$, before the stimulus, and one part $(x_s(t), y_s(t))$, $t \in [\varphi T_0, T_1]$, after the stimulus, where T_1 denotes the period of the perturbed cycle. These two trajectories are then followed simultaneously by effectively considering a four-dimensional system in which the first two dimensions contain the first part and the last two dimensions the second part.

A boundary value problem then models the cycle and the discrete perturbation, where the system of differential equations is given by

$$\begin{aligned}
\dot{x}_\Gamma &= \frac{1}{\varepsilon}(-y_\Gamma - x_\Gamma^3 + a^2 x_\Gamma),\\
\dot{y}_\Gamma &= \varepsilon(b x_\Gamma - y_\Gamma),\\
\dot{x}_s &= \frac{1}{\varepsilon}(-y_s - x_s^3 + a^2 x_s),\\
\dot{y}_s &= \varepsilon(b x_s - y_s),
\end{aligned}$$

and the boundary conditions are given by

$$\begin{aligned}
x_\Gamma(0) &= x_0,\\
y_\Gamma(0) &= y_0,\\
x_s(\varphi T_0) &= x_\Gamma(\varphi T_0) + \Delta x,\\
y_s(\varphi T_0) &= y_\Gamma(\varphi T_0),\\
y_s(T_1) &= y_1.
\end{aligned}$$

Here $(x_0, y_0) = (1.41589, 0) \in \Gamma$ denotes the fixed starting point on the cycle, $T_0 = 22.4869$ the period of the cycle, and y_1 the y-coordinate of the endpoint, which is allowed to vary for intermediate continuation steps that do not compute the phase transition curve but is fixed

as $y_1 = 0$ otherwise. Note that for $\Delta x = 0$ there is no perturbation, and hence $T_0 = T_1$, but φ can still vary.

The cycle is extremely attracting, with the magnitude of the nontrivial Floquet multiplier less than 10^{-80}, so constraining the y-coordinate of the endpoint for positive x is sufficient for the endpoint to be close to the starting point (x_0, y_0). While continuing this system in φ, the phase transition curve can be monitored by computing $g(\varphi) = \varphi + (T_0 - T_1(\varphi))/T_0$.

To be able to fit the boundary value problem into AUTO, both segments must be scaled and translated in time from the intervals $[0, \varphi T_0]$ and $[\varphi T_0, T_1]$ to the interval $[0, 1]$. Such transformations give rise to the system of differential equations

$$\begin{aligned}
\dot{x}_\Gamma &= \varphi T_0 \frac{1}{\varepsilon}(-y_\Gamma - x_\Gamma^3 + a^2 x_\Gamma),\\
\dot{y}_\Gamma &= \varphi T_0 \varepsilon(b x_\Gamma - y_\Gamma),\\
\dot{x}_s &= (T_1 - \varphi T_0)\frac{1}{\varepsilon}(-y_s - x_s^3 + a^2 x_s),\\
\dot{y}_s &= (T_1 - \varphi T_0)\varepsilon(b x_s - y_s),
\end{aligned}$$

subject to the boundary conditions

$$\begin{aligned}
0 &= x_\Gamma(0) - x_0,\\
0 &= y_\Gamma(0) - y_0,\\
0 &= x_s(0) - x_\Gamma(1) - \Delta x,\\
0 &= y_s(0) - y_\Gamma(1),\\
0 &= y_s(1) - y_1.
\end{aligned}$$

The continuation strategy is then as follows.

1. Set $(x_\Gamma(t), y_\Gamma(t)) = (x_0, y_0)$ and $(x_s(t), y_s(t)) = (x_0 + \Delta x, y_0)$ for all t and $y_1 = \varphi = T_1 = 0$.
2. Continue in T_1 and y_1 until $y_1 = 0$ for the third time. This effectively grows the orbit $(x_s(t), y_s(t))$ from the point $(x_0 + \Delta x, y_0)$ corresponding to the initial stimulus applied at (x_0, y_0) until it returns close to the stimulus point.
3. Continue in φ and T_1 until $\varphi = 1$, constraining the endpoint so that $y_s(1)) = y_1 = 0$. The orbit segment $(x_\Gamma(t), y_\Gamma(t))$ before the stimulus is applied now grows from the point (x_0, y_0), and the stimulus point $(x_\Gamma(1), y_\Gamma(1))$ corresponds to and varies with the endpoint of this first part. The phase transition curve can be directly computed. This strategy works only if the phase transition curve is continuous; if the curve is discontinuous, and the segment $(x_s(t), y_s(t))$ crosses a saddle equilibrium point, then T_1 will tend to infinity at a certain phase. Then, we must split this step into three parts:
   (a) Continue in φ and T_1 until $T_1 = T_{\max}$. Here $T_{\max}$ must be sufficiently high to ascertain the discontinuity.
   (b) Continue in φ and y_1, fixing the integration time T_1, until $y_1 = 0$ again, to reach the other side of the saddle. During this intermediate calculation, the phase transition curve is not well defined.

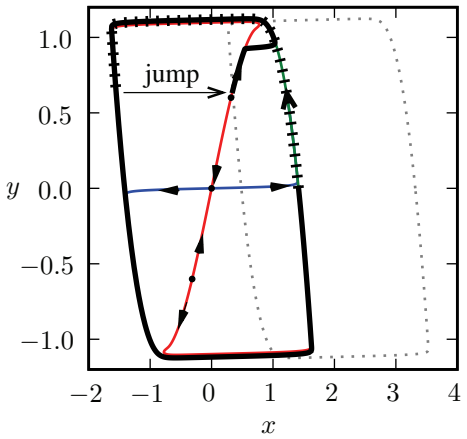

Figure 3. *Phase space as in Figure 2 with shifted orbits and critical trajectories added. The shifted cycle is perturbed by $\Delta x = 1.9$. The hatched trajectory makes a jump of $\Delta x = 1.9$ and continues as the thick black trajectory along the weak unstable manifold for a long time in a canard-like trajectory until converging back to the cycle. The dotted gray cycle denotes the shifted cycle.*

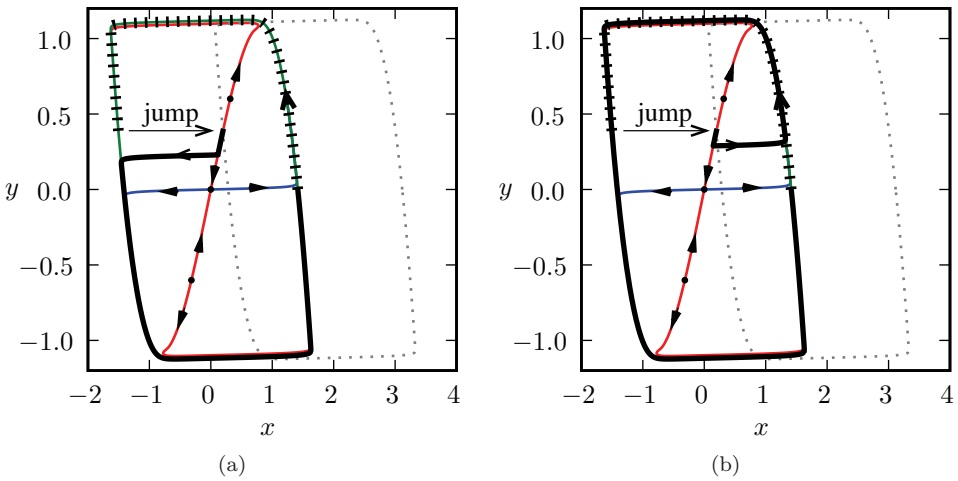

Figure 4. *Phase space as in Figure 3 where the shifted cycle is now perturbed by $\Delta x = 1.7$. The hatched trajectory makes a jump of $\Delta x = 1.7$ and continues as the thick black curve along the stable manifold of the saddle for a long time before converging back to the cycle, either moving to the left (panel* (a)*, before the discontinuity) or moving to the right (panel* (b)*, after the discontinuity).*

(c) For the remainder of the continuation, proceed as in step 3 above.

The above procedure was applied for two values of Δx: 1.9 and 1.7. For $\Delta x = 1.9$, the phase transition curve is continuous. However, the perturbed cycle can follow the weak unstable manifold of the saddle for a long time in a canard-like trajectory, giving rise to a transient up to $T_1 = 6.2971T_0$. For $\Delta x = 1.7$, the saddle interferes, and we use a value of $T_{\max} = 7T_0$. The structure of these extreme perturbed trajectories can be seen in Figures 3 and 4.

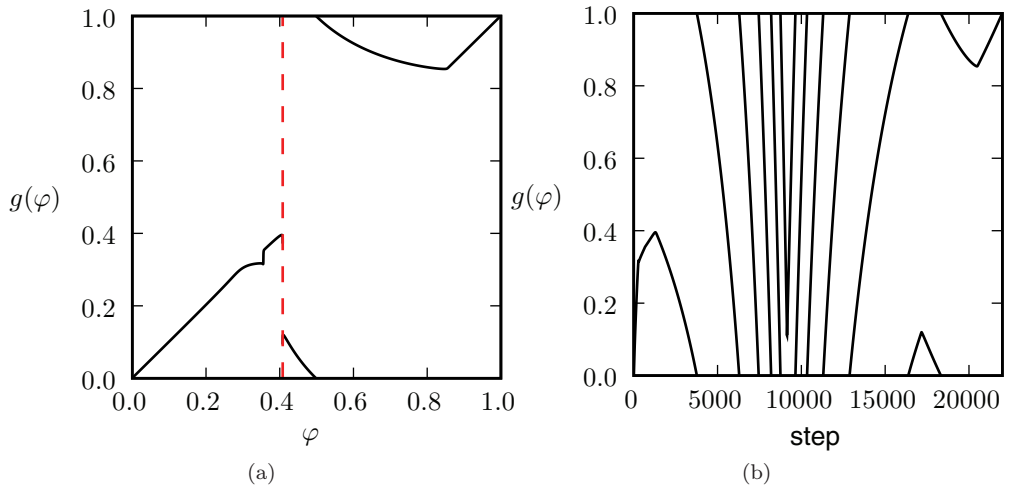

Figure 5. (a) *Plot of the phase transition curve for* (3.1) *using the constrained end state method for a perturbation of* $\Delta x = 1.9$*, which leaves the state point always in the basin of attraction of the limit cycle. The horizontal axis denotes the phase at which the perturbation occurs. The red dashed line shows the apparent discontinuity, that is, the part that was found using continuation but not using shooting techniques.* (b) *The same curve as* (a)*, but now the horizontal axis denotes the continuation step. This shows the fine structure of the resetting.*

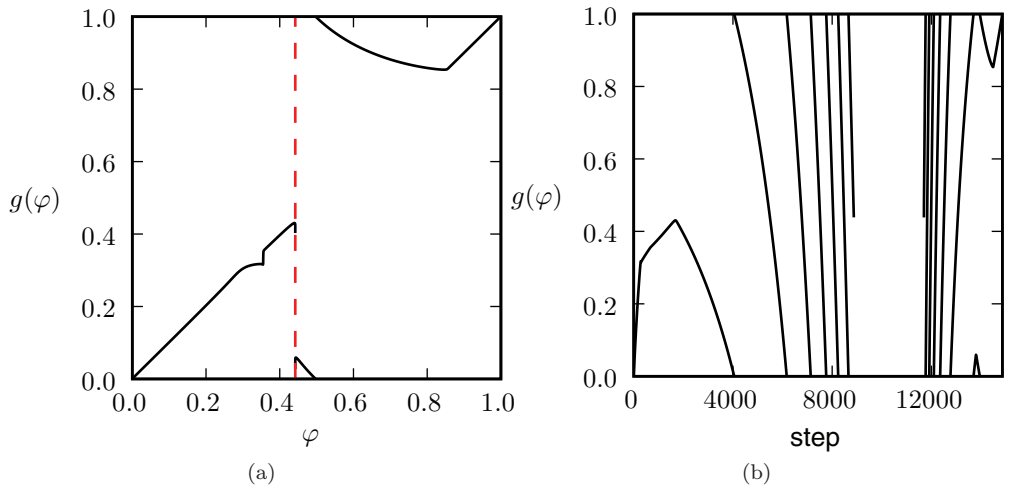

Figure 6. (a) *Plot of the phase transition curve for* (3.1) *for a perturbation of* $\Delta x = 1.7$*, as in Figure* 5(a)*. Here a combination of the constrained end state and fixed time methods was used. The state point is moved out of the basin of attraction of the limit cycle to the stable manifold of the saddle.* (b) *The horizontal axis denotes the continuation step, as in Figure* 5(b)*; the gap corresponds to the fixed time continuation interval during which the phase transition curve cannot be obtained.*

Note that the maximum $T_1 = 6.2971T_0$ is a limit point in the continuation procedure, which could be continued in the three parameters φ, T_1, and Δx. That would allow us to compute the boundary of the continuity region of the phase resetting curve.

The resulting phase transition curves are shown in Figures 5(a) and 6(a). Note the striking

similarity. If, instead of continuation, a shooting method were used, the figures would look qualitatively the same (the apparently vertical red dashed line at the critical phase would be missing), and one could easily conclude that a discontinuity appears in both cases. However, using continuation the difference of the orbit in both phase space and parameter space is taken into account.

To be more specific, given an existing orbit $\mathbf{u}$ at parameter values $\mathbf{p}$, and a continuation direction $(\mathbf{u}', \mathbf{p}')$, the next orbit for step size Δs in the continuation is predicted to be at $(\mathbf{u}, \mathbf{p})_{\text{new}} = (\mathbf{u}, \mathbf{p}) + \Delta s(\mathbf{u}', \mathbf{p}')$ and then corrected using Newton iterations in a process called pseudo-arclength continuation. A new value for the continuation direction can then be computed by subtracting the corrected new and old orbits. The step size is automatically adapted depending on the number of Newton iterations necessary to converge and is allowed to vary between the two specified values $\Delta s_{\min}$ and $\Delta s_{\max}$.

Hence, to analyze the complete phase transition curve, we also provide plots versus the continuation step number. Even though the continuation step size may be adapted during continuation and the relationship between φ and the step is highly nonlinear, the qualitative structure of the phase transition curve immediately becomes clear. Such plots are provided in Figures 5(b) and 6(b). The gap in Figure 6(b) corresponds to the discontinuity, where the number of continuation steps in the gap corresponds to step 3(b) described above.

4. Resetting a pacemaker in an excitable medium. In this section we consider resetting a pacemaker embedded in an excitable medium with one spatial dimension. Pulses of activation generated at the pacemaker site propagate through the surrounding medium, resulting in a periodic train of one-dimensional expanding target patterns emanating from the pacemaker site. Although it is usual to assume that cardiac tissue is well described by an appropriate partial differential equation, in some circumstances the discrete cellular nature of cardiac tissue appears important [37, 20, 8, 21, 33, 22, 32]. As such, we consider two different spatial discretizations: one of which approximates the continuous nonlinear partial differential equation, and one more suitable to a coarsely discretized system.

Since we are motivated by cardiac systems, we adapt the FitzHugh–Nagumo equation to represent a line of excitable medium with an embedded pacemaker [19]. As described in earlier work [31, 27], the FitzHugh–Nagumo equations can support both low amplitude unstable slow waves, designated S (or s), and high amplitude stable fast waves, designated F (or f), where lower case letters represent waves propagating to the left and upper case letters represent waves propagating to the right.

We consider the system of partial differential equations

$$\begin{aligned} v_t &= \frac{1}{\varepsilon}(v - v^3 - w) + I_s + I_p + Dv_{xx}, \\ w_t &= \varepsilon(v + \beta - \gamma w)\left(\frac{w_h - w_l}{1 + e^{-4v}} + w_l\right), \end{aligned} \tag{4.1}$$

where x is measured in centimeters and t is in units of 10 milliseconds, because this is a model of a cardiac system. The variable $v(x,t)$ is an excitation variable, $w(x,t)$ is a recovery variable, $\beta = 0.7$, $\gamma = 0.5$, $\varepsilon = 0.3$, $D = 1$, $I_s(x,t)$ is a stimulation variable, and $I_p(x)$ is a pacemaker current. The constants w_l and w_h control the duration of the recovery phases and

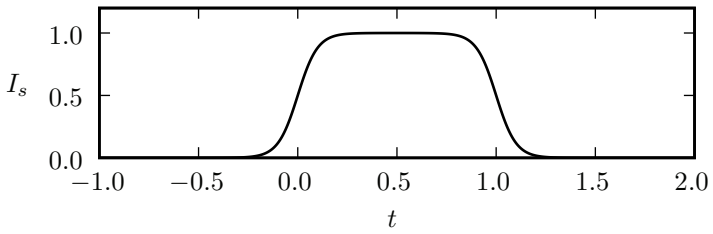

Figure 7. *The stimulus function I_s (4.2) for $\varphi = 0$ that approximates a square wave.*

the active states of the excitable medium. The pacemaker oscillator is modeled by changing I_p and w_l in the pacemaker region:

$$\begin{cases} \text{pacemaker: } 0.72 \le x \le 0.76 & : I_p = 1, w_l = 0.13, \\ \text{elsewhere (excitable regions)} & : I_p = 0, w_l = 0.4. \end{cases}$$

We apply a stimulus I_s of the form

$$I_s = A(\tanh(10(t - t_s)) - \tanh(10(t - t_e)))/2 \tag{4.2}$$

so that it approximates a square pulse; see Figure 7. The stimulus is applied at $x \le 0.02$ for a duration $t_e - t_s = 1$. The start time t_s is varied to control the phase of stimulation $\varphi = t_s/T_0$, and the stimulus amplitude A is initially fixed at 1. The resulting phase $g(\varphi)$ is measured at the pacemaker at $x = 0.74$ as the time at which the first regular maximum of v occurs, divided by T_0, and then shifted so that $g(0) = 0$.

The boundary conditions consist of Dirichlet boundary conditions at $t = 0$, that is, fixed initial conditions, and Neumann conditions at $x = 0$ and $x = L = 0.84$:

$$v(x, 0) = v_0(x), \quad w(x, 0) = w_0(x), \tag{4.3}$$

$$v_x(0, t) = 0, \quad w_x(0, t) = 0, \tag{4.4}$$

$$v_x(L, t) = 0, \quad w_x(L, t) = 0. \tag{4.5}$$

We first discretize (4.1) on a lattice of 43 cells using an 87-dimensional (including t) continuous system of ordinary differential equations involving $v_1, \ldots, v_{43}$, $w_1, \ldots, w_{43}$, and t, where $v_i = v_i(t)$, $w_i = w_i(t)$, $x = dx(i - 1)$, with $dx = 0.02$, and $\dot{t} = 1$, using a 4th-order compact Collatz "Mehrstellen" scheme [5] to estimate $\nu_i = (v_{xx})_i$:

$$\begin{aligned} (2\nu_2 + 10\nu_1)/12 &= 2(v_2 - v_1)/dx^2 \quad \text{for } i = 1, \\ (\nu_{i+1} + 10\nu_i + \nu_{i-1})/12 &= (v_{i+1} - 2v_i + v_{i-1})/dx^2 \quad \text{for } 2 \le i \le 42, \\ (10\nu_{43} + 2\nu_{42})/12 &= -2(v_{43} - v_{42})/dx^2 \quad \text{for } i = 43. \end{aligned} \tag{4.6}$$

We integrate the system using the 4th-order Dormand–Prince method [10] up to $t = T = 250$ so as to use accurate 4th-order schemes throughout, that is, for both the space and time discretizations, to obtain a state (v^*, w^*) that lies on a limit cycle oscillation with

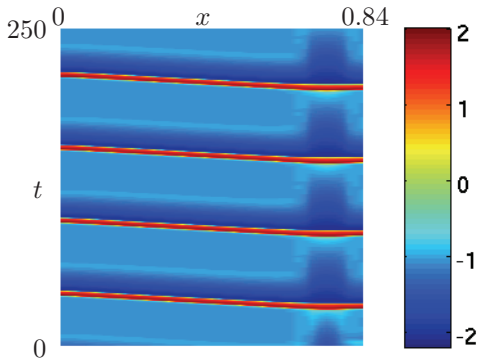

Figure 8. *Space-time plot for v in the FitzHugh–Nagumo system (4.1), where the applied stimulus $I_s = 0$.*

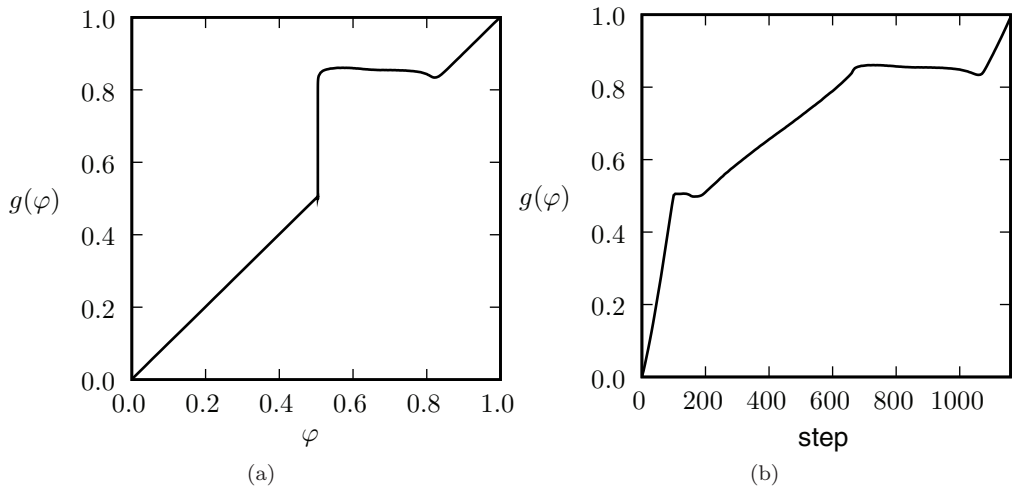

Figure 9. (a) *Phase transition curve for an apparent discontinuity in the FitzHugh–Nagumo system (4.1), where $A = 1$ and $dx = 0.02$.* (b) *Here the horizontal axis denotes the continuation step.*

$T_0 \approx 57.353757$. The resulting space-time diagram for $A = 0$, that is, without the stimulation I_s applied, is depicted in Figure 8. We then use this state as an initial condition for the resetting runs.

We first used Dormand–Prince integration and shooting methods to compute the resetting curve, as in Figure 9(a). This shows three ranges of phase with distinct behaviors and resetting features:

1. $0 \le \varphi \le \varphi^* \approx 0.504$. In this range the stimulus generates a large amplitude stable fast pulse, F, which collides with a wave generated by the pacemaker, as can be seen in Figure 10(a), or falls in the refractory period of the tissue and fails to elicit a wave that propagates to the pacemaker, as in Figure 10(b). In either case the stimulus has no effect on the pacemaker, and consequently $g(\varphi) = \varphi$.
2. $\varphi^* < \varphi < 0.82$; see Figures 10(e) and (f). For this range of phases the stimulus generates a fast pulse, F, that propagates to the pacemaker and resets it. The first

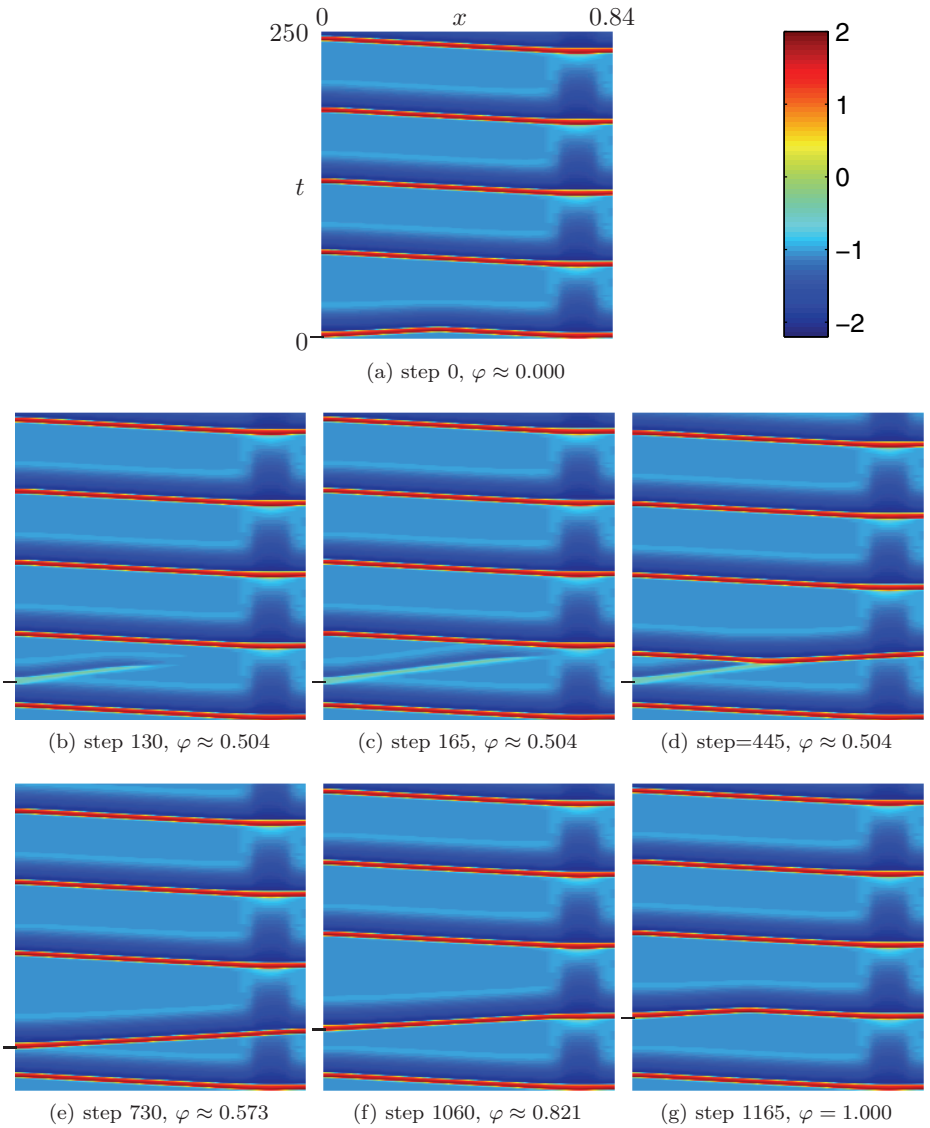

(a) step 0, $\varphi \approx 0.000$

(b) step 130, $\varphi \approx 0.504$ (c) step 165, $\varphi \approx 0.504$ (d) step=445, $\varphi \approx 0.504$

(e) step 730, $\varphi \approx 0.573$ (f) step 1060, $\varphi \approx 0.821$ (g) step 1165, $\varphi = 1.000$

Figure 10. *Space-time plots for v in the FitzHugh–Nagumo system (4.1), where "step" denotes the continuation step number. Here the phase of the stimulus is shifted with respect to panel* (a)*, $A = 1$, and $dx = 0.02$. The tick marks along the left-hand sides of the plots mark the time at which the stimulus I_s is applied. Panels* (b), (c), (e), *and* (f) *correspond to extrema in Figure 9*(b)*. Intermediate panel* (d) *shows the pattern SfF most clearly. The accompanying movie (see* 81922_01.avi [local/web 1.35MB]*) shows the sequence* (a)–(f) *as a continuous process.*

instance of resetting around φ^* causes an apparent jump discontinuity in the phase transition curve. In this range, $g(\varphi) \approx 0.82$.

3. $0.82 < \varphi < 1.0$; see Figure 10(g). For all stimulus phases in this range the induced fast pulse collides with a wave emitted by the pacemaker so that there is no resetting. In this range, $g(\varphi) = \varphi$.

We can estimate these ranges by using a simple model of excitable media with refractory period R, in which waves propagate with velocity c, the pacemaker has the period T_0 [14], and the stimulus is at a distance d from the pacemaker. In our computation $R \approx 18.6$, $d \approx 0.74$, $v \approx 0.067$, and $T_0 \approx 57.4$. For this model we find $\varphi^* = (R+d/c)/T_0$. Furthermore, the level of the plateau in Figure 9 is $g(\varphi) = (T_0 - d/c)/T_0$. In the current situation we estimate $\varphi^* \approx 0.51$ and the value of $g(\varphi) \approx 0.81$ for the plateau. The small discrepancies from these values in the computations arise from nonlinear effects such as the variable velocity in the medium following an excitation. In the case that the stimulus is given at distance $d > c(T_0 - R)/2$, the stimulus will fail to reset the pacemaker for all phases of delivery.

After this jump $g(\varphi) \approx 0.85$ stays relatively constant with respect to φ. The resetting in this region can be estimated by $g(\varphi) = 1 - (R + t_d)/T_0$, where R is the refractory period of the medium and t_d is the delay associated with the propagation from stimulus to pacemaker site.

Note that all the figures described above were in fact obtained using continuation but looked the same using shooting methods.

To probe the apparent discontinuity at φ^* we carry out a continuation using the fixed integration time method in [9], using a boundary value problem where the solution is fixed at $t = 0$, and the integration time is fixed at $T = 250$. This amounts to the 87-dimensional ordinary differential equation given by (4.1) discretized using (4.6) plus $\dot{t} = 1$, subject to a total of 87 boundary conditions, (4.3) plus $t(0) = 0$. Such a continuation problem is consistent when there is only one free parameter; in this case we vary only φ, which is equivalent to varying t_s. The endpoint is completely left alone. This technique corresponds to continuation step 3(b) in section 3, except that in this case the equivalent of y_1 is not explicitly tracked.

As can be seen in Figure 10, when φ increases from φ^*, the stimulus generates an unstable slow wave, S, which splits into two counterpropagating fast waves, f and F; see Figure 10(d). We label this type of solution SfF and note that similar reflected pulse solutions have previously been seen by others using a range of different excitable equations [11, 7, 2, 4]. At slightly later phases Figure 10(e) shows that the stimulus elicits a single fast pulse F leading to full resetting, where $g(\varphi) \approx 0.861$.

Figure 9(b) shows the fine structure of the phase resetting expanded around the sharp transition at φ^*. This critical phase φ^* is encountered around step 130, at which point the slow unstable wave S is generated at the stimulus site and propagates farther to the right with each continuation step until it almost reaches the pacemaker site in Figure 10(b). Just beyond this point the pacemaker begins to experience a small delay in its firing due to the influence of the slow wave S, which corresponds to the small decrease in the phase transition curve between steps 130 and 165; see Figure 10(c). When the slow pulse S propagates sufficiently close to the pacemaker the SfF solution appears, with the split from S to fF occurring at the pacemaker site. At around step 170 the SfF split site begins to move left toward the stimulus site, as shown in Figure 10(d), incrementally advancing the resultant phase of the pacemaker. When the SfF split site reaches the stimulus site, around step 730, the S and f pulses disappear, and what is left is the fast pulse F resetting the pacemaker as shown in Figure 10(e).

To complement these observations we also look at the phase resetting caused by varying the stimulus amplitude A at $\varphi \approx 0.509$, a value slightly higher than φ^*, from 0 to 1. As

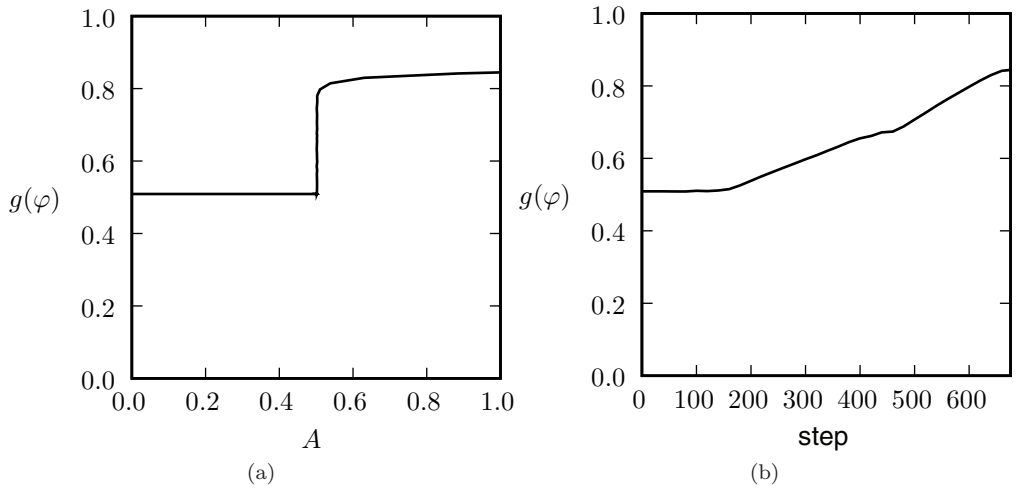

Figure 11. (a) *Phase resetting caused by varying the stimulus amplitude A for the FitzHugh–Nagumo system (4.1), where $dx = 0.02$ and $\varphi \approx 0.509$. Note how $g(\varphi)$ moves from 0.509 to 0.845, corresponding to the point $(\varphi, g(\varphi)) \approx (0.509, 0.845)$ in Figure 9.* (b) *Here the horizontal axis corresponds to the continuation step. The behavior in space-time for this process, following a sequence similar to the panels in Figure 10, is shown in the accompanying movie (see* 81922_02.avi [local/web 351KB]*). Note how the first frame in this movie equals the basic state in Figure 8 where $A = 0$.*

shown in Figure 11(a), there is a sharp transition to resetting following a stimulus of amplitude $A \approx 0.502$. At the transition the jump in $g(\varphi)$ from 0.509 to 0.845 is similar to what is seen around φ^* in the phase resetting experiment. The transition from no propagation, via S and SfF, to F is also observed in this amplitude continuation. The main difference between using the phase and using the amplitude for resetting is that the slow wave generated at the stimulus site is not able to reach the pacemaker site and cause the small phase advances seen during steps 130–165 of the stimulus phase continuation. This is due to the fact that the slow wave begins to propagate from the stimulus site slightly later relative to the time in the phase resetting experiment, which happens because the stimulus is applied for a nonzero duration. Nevertheless, the continuity of the phase transition curve is preserved under amplitude continuation at $\varphi \approx 0.509$, which is in concordance with the Continuity Lemma, Lemma 2.1.

We found that a different resetting scenario occurs varying the amplitude for a coarser discretization of space ($dx = 0.04$). Analysis of the propagation parameters at different mesh discretizations showed appreciable change of action potential duration, maximal rate of activation, and propagation velocity between the discretizations $dx = 0.02$ and 0.04. In contrast, comparing $dx = 0.02$ with the even finer discretization $dx = 0.01$ showed much smaller variations ($< 2\%$ for propagation velocity, activation duration, and maximal rate of activation). Together these observations corroborate the fact that the coarser discretization $dx = 0.04$ can have different properties than the continuous partial differential equation (4.1).

A very fine discretization is too computationally expensive for the continuation methods that we used. Because AUTO employs Gauss elimination to solve the linearized system during Newton iterations, halving dx causes an increase of up to a factor of 8 in the computation time of AUTO. With a space discretization where $dx = 0.02$ we already needed several hours

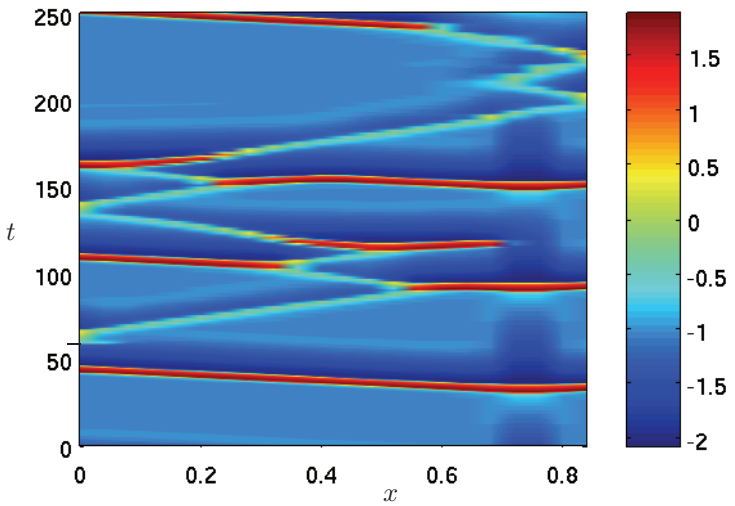

Figure 12. *Space-time plot for v in (4.1) on a coarse grid with $dx = 0.04$. During the continuation this situation corresponds to the first time that the waves caused by the stimulus reach $t = 250$. The phase is at $\varphi \approx 0.509$; the amplitude is at the critical value $A \approx 0.502$. The accompanying movie (see* 81922_03.avi [local/web 11.8MB]*), varying the amplitude A, shows how this situation is obtained from the basic state in Figure 8 and also shows a limited further continuation.*

on a cluster using 16 processors in parallel.

The gross features of the phase transition curve for the coarse case are very similar to those of the finely discretized case shown in Figure 11(a). However, looking closely around the apparent jump discontinuity at $A \approx 0.502$ using continuation, we find differences in the fine structure of the phase transition curve at $dx = 0.04$. The algorithm begins to track solutions which are not present in the $dx = 0.02$ case, so the discretization no longer approximates the continuous partial differential equation sufficiently. We observed trajectories consisting of a slow wave S either (a) reflecting from the boundary, or (b) splitting into an anterograde fast wave F and a retrograde slow wave s. The slow wave s can reflect or split another slow wave S multiple times as shown in Figure 12. The sequence of slow pulse reflections begins to look like an extremely complex solution where the pacemaker never reestablishes entrainment of the medium, and so the system is taken out of the basin of attraction $B(\Gamma)$.

In Figure 12 the initial range of times shows the slow wave S hitting the fast wave around $t = 90$ at cell 15 ($x = 0.56$), much like in Figure 10(b). However, the wave now splits into an anterograde fast pulse F and retrograde slow wave s at a point distant from the pacemaker site. The continuation shows a complex recursive interaction of fast wave stubs with slow waves, where fast waves grow or shrink one cell at a time. Eventually the fast wave around $t = 90$ grows to cell 14 ($x = 0.52$), then to cell 13 ($x = 0.48$), and so on, up to cell 5 ($x = 0.16$). Beyond cell 5 the procedure arrives at a situation similar to Figure 10(d) and then continues to Figure 10(e) in a straightforward fashion. The time values of the maxima at cell 11 ($x = 0.4$) for a continuation up to $t = 125$ are tracked in Figure 13. Before continuation step 60000, there exist two slow waves, one starting around $t = 100$ and one starting around

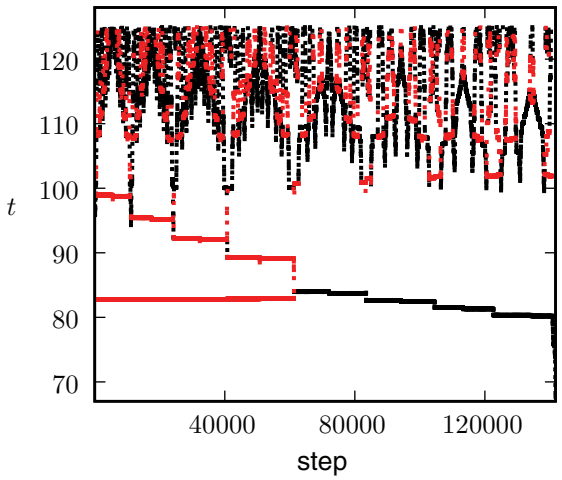

Figure 13. *Tracking time values of the maxima of v at cell 11 ($x = 0.4$) versus continuation step on a coarse grid with $dx = 0.04$, $T = 125$, where the amplitude A varies. Black points denote maxima of fast waves and red points maxima of slow waves. The accompanying movie (see* 81922_04.avi [local/web 24.1MB]*) shows the corresponding complete continuation in space-time: note how the first 2.3 seconds of this movie are identical to the first 9 seconds of the partial movie (see* 81922_03.avi [local/web 11.8MB]*) for $T = 250$ attached to Figure 12. After this initial part the lower half for $t < 125$ no longer changes. The movie for $T = 250$ never reaches any corresponding further point in the movie for $T = 125$ because that is too computationally expensive.*

$t = 83$. The wave for $t = 100$ moves a little each time as the fast wave grows one cell. Around continuation step 60000, that is, at the fourth bump, the fast wave has grown to cell 11 and the two reflected slow waves are merged into the fast wave.

The main problem with dissecting the full sequence of phase transitions in the $dx = 0.04$ case is the extremely long computation time required to make it through the continuation, as evidenced by the number of steps in Figure 13. Continuing for $T = 125$ took around a week; higher values quickly become prohibitively expensive by an estimated factor of 1.85 for every additional 5 time units, because of the recursive nature of the structure. Hence the movie for $T = 250$, referred to in Figure 12, shows only a partial continuation, where the initial part for $t < 125$ follows only the first 35 frames (2.3 seconds) of the movie for $T = 125$.

Nevertheless, the fact that the multireflected unstable slow wave disappears at finer dx implies that the solution is inherent to the discretized system of coupled ordinary differential equations rather than the continuous partial differential equation. Regardless, this solution need not be interpreted as a numerical artifact since, as mentioned previously, there are cases for which the continuous cable equation fails to hold in models of cardiac tissue.

5. Resetting a pacemaker in a system governed by the Morris–Lecar equations. In this section we provide an example of a partial differential equation where the phase transition curve is discontinuous, through a mechanism involving a one-dimensional spiral wave solution that was studied, but not applied to phase transition curves in [7]. It is given by the

Table 1
Morris–Lecar parameters used in (5.1).

D	g_l	g_K	g_{Ca}	v_1	v_2	v_3	v_4	E_{Ca}	E_K	E_l	ε	I_{app}
0.001	2	8	4.4	−1.2	18	2	10	120	−84	−60	0.18	10

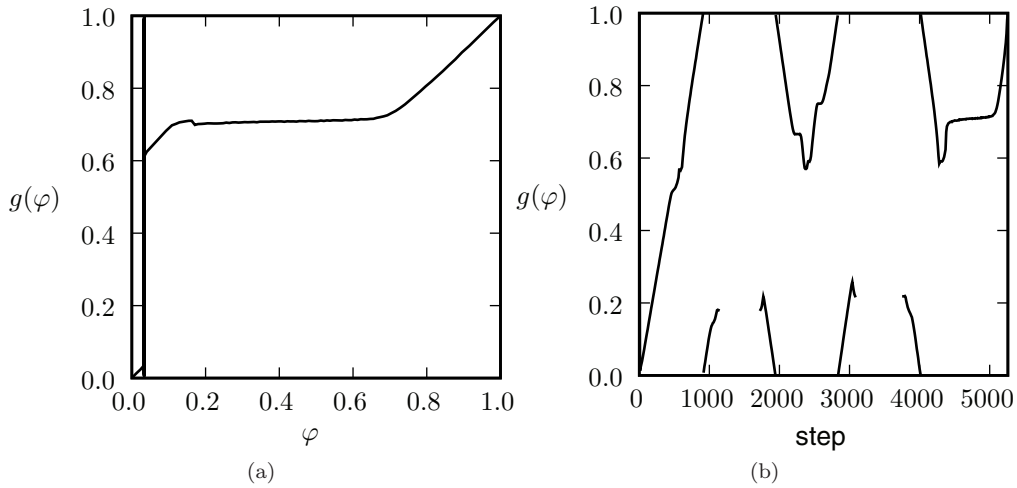

Figure 14. (a) *Phase transition curve for the Morris–Lecar system (5.1), measured at the pacemaker at* $x = 0.165$. (b) *Here the horizontal axis denotes the continuation step.*

Morris–Lecar system of partial differential of equations

$$
\begin{aligned}
m_\infty(v) &= \left(1 + \tanh\left(\frac{v - v_1}{v_2}\right)\right)/2, \qquad v_\infty(v) = \left(1 + \tanh\left(\frac{v - v_3}{v_4}\right)\right)/2,\\
\tau(v) &= 1/\cosh\left(\frac{v - v_3}{2v_4}\right),\\
v_t &= -g_{Ca} m_\infty(v)(v - E_{Ca}) - g_K w(v - E_K) - g_l(v - E_l) + I_{\text{app}} + I_s + D v_{xx},\\
w_t &= \varepsilon \frac{v_\infty(v) - w}{\tau(v)},
\end{aligned}
\tag{5.1}
$$

with parameters given in Table 1.

For this example, we use the same algorithm and discretization scheme as in section 4, but with different parameters. The discretization now uses 41 equally spaced mesh points in space over the x-interval $[0, 0.2]$, so $dx = 0.005$. The mesh points corresponding to the x-interval $[0.15, 0.185]$ correspond to the pacemaker, with a modified applied current of $I_{\text{app}} = 60$. We use Neumann boundary conditions, and the total time interval has length 36.

At the x-interval $[0.04, 0.055]$ we apply a stimulus I_s of the form

$$I_s = A(\tanh(10(t - t_s)) - \tanh(10(t - t_e)))/2,$$

where $A = 2700$ and $t_e = t_s + 0.06$, where t_s varies. The resulting phase transition curves and space-time diagrams are shown in Figures 14 and 15.

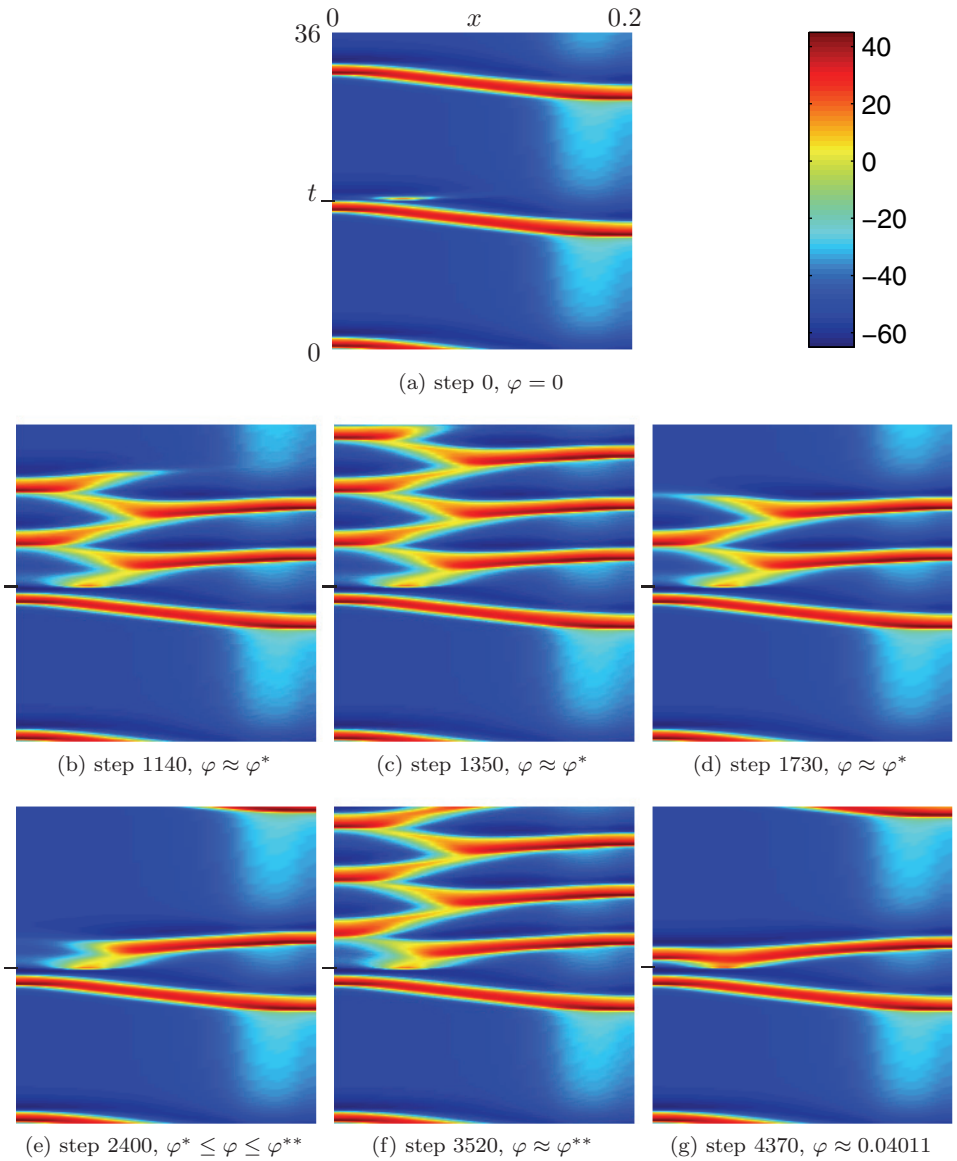

(a) step 0, $\varphi = 0$

(b) step 1140, $\varphi \approx \varphi^*$ (c) step 1350, $\varphi \approx \varphi^*$ (d) step 1730, $\varphi \approx \varphi^*$

(e) step 2400, $\varphi^* \le \varphi \le \varphi^{**}$ (f) step 3520, $\varphi \approx \varphi^{**}$ (g) step 4370, $\varphi \approx 0.04011$

Figure 15. *Space-time plots for v in the Morris–Lecar system (5.1), where $\varphi^* \approx 0.03343$ and $\varphi^{**} \approx 0.03347$.* (a) *The stimulus does not propagate.* (b) *Building the first one-dimensional spiral ($ffFF$).* (c) *The first one-dimensional spiral (the start $fffFFF$ is observed).* (d) *Destroying the first one-dimensional spiral (fFF).* (e) *Single propagating fast wave F.* (f) *Second one-dimensional spiral (the start $fffFFF$ is observed).* (g) *Double fast wave fF. The accompanying movie (see* 81922_05.avi [local/web 2.39MB]*) shows how these plots continuously connect to each other, in the same spirit as in Figure 10.*

At first sight, Figure 14(a) shows a single apparent discontinuity. We used continuation techniques to investigate this and found that the one-dimensional spiral solution appears twice. We also used shooting techniques to investigate this system, as was done in [7]. However, using shooting only the very beginning of the one-dimensional spiral can be found, whereas using

continuation we could in principle, given enough resources, reproduce as much of this structure as is desired and produce a continuous movie. The shooting ability also allowed us to confirm the validity of the structure with a finer discretization in space, which is computationally much cheaper than using continuation.

In Figure 15, starting from the state in panel (a), where the stimulation dies out much like in Figure 10(b), as the phase of the stimulus increases, a one-dimensional spiral grows in qualitatively the same way as described in [7]. As the phase increases further, the spiral shrinks again until we arrive at the situation seen in panel (e), where the stimulus gives rise to a single fast wave F propagating to the right. Upon further increasing, a new one-dimensional spiral appears in panel (f), which then breaks down again, and eventually we are left with fast waves propagating both to the left and to the right from the stimulus in panel (g). After this the situation gradually moves back to the one in Figure 14(a), shifted by one phase, in a continuous fashion. Note that the phase in the movie is shifted by $\Delta\varphi \approx 0.96144$, so the latter part of this description applies to the first part of the movie.

In the phase transition curve in Figures 14(b) there are two gaps, from steps 1140 to 1730 and from steps 3080 to 3770, corresponding to the places where the spiral appears. Because we integrated up to a fixed time, for those gaps it is not possible to reliably compute the phase transition curve. Figures 14(b) and 14(d) correspond to the boundaries of the first gap.

In other numerical experiments, not discussed in detail here, we found that for smaller values of the applied current such as $A = 2500$ for the stimulus, the one-dimensional spiral does not appear at all, and the transition is like that for the FitzHugh–Nagumo system in section 4. In other words, using the notation of [7], for a stimulus of $A = 2700$ the rest/fast wave (R/F) threshold is crossed twice, from R to F and back to R, but for smaller A it is not crossed at all and stays at R. This observation serves to further reinforce the thin line between real and apparent discontinuity of phase transition curves.

6. Discussion.

This paper analyzes resetting of oscillators that are localized to some region of excitable space. For neural and cardiac systems, which motivated the current studies, stimuli will typically have to travel through excitable tissue before resetting is elicited. Consider for example, an intact heart in which an excitation from the normal (sinus) pacemaker resets a pacemaker at an abnormal (ectopic) location, or in which an inserted artificial pacemaker interacts with sinus or ectopic rhythms.

Previous work has indicated that propagation solutions can have a very sensitive dependence on stimuli parameters for stimuli delivered during the transition of tissue from a refractory to an excitable state (often called the vulnerable period) [19, 38, 13, 26, 25, 7]. This phenomenon can manifest itself as an apparent jump discontinuity in the phase transition curve. In order to tease out the fine structure of the resetting around these jumps in the phase transition curve, we have adapted continuation methods [9]. For the cases analyzed, we find that the continuity properties of the phase transition curve are consistent with mathematical results which indicate that unless stimuli lead to a transition outside the basin of attraction of an oscillator, the transition curves will be continuous. For situations in which a stimulus leads to transitions outside the basin of attraction of an oscillator, constrained end state continuation methods will fail to estimate the phase transition curve. This work therefore provides a new operational method to detect the existence of transitions outside the basin

of attraction of the oscillation. This is true regardless of whether the discontinuous transitions originate from the pacemaker itself (like the stable manifold of the saddle in the Van der Pol example in section 3) or from a spatially periodic solution in the excitable media away from the pacemaker site, like the one-dimensional spiral in section 5. Further, the methods should be applicable to other situations, such as a rotating wave on a one-dimensional ring with a tail, in which discontinuous resetting was observed even though all stimuli left the system in the basin of attraction of the rotating wave [25].

Although we restricted our attention to systems in one spatial dimension, the continuation methods used here should be adaptable to analysis of resetting in excitable media of higher dimensions. It should be possible to use continuation methods to analyze resetting a pacemaker in higher spatial dimensions. This may provide new ways to investigate and generate solutions outside of the basin of attraction of attraction of the pacemaker, such as spiral waves in two dimensions and scroll waves in three dimensions [40]. Such extensions of this work will be challenging in view of the high dimensions that would be needed to approximate the spatially distributed system by ordinary differential equations.

This work primarily deals with theoretical questions and methodologies that do not appear related to practical situations, since they occur over such small ranges of parameter space. However, experimental studies of propagation of cardiac excitation in one-dimensional cardiac Purkinje fibers show some strikingly similar behaviors in which echo waves can be generated in vitro [1, 3]. A rare clinical condition called bidirectional ventricular tachycardia has been hypothesized to arise from alternating conduction down Purkinje fibers muscle fibers (technically these are the right and left fascicles of the left bundle branch) originating from a single focus [30]. Based on the current work, we suggest that one-dimensional spiral waves originating at the junction point would be a potential dynamical mechanism that could lead to such behavior.

A number of rigorous results exists on the behavior of one-dimensional spirals in pacemakers, for example, in [34, 35], where they are referred to as spiral defects. It is interesting, but beyond the scope of this paper, to link these results to those presented here. The qualitative explanation of the one-dimensional spiral as a global bifurcation in [7] applies here, too.

The current work demonstrates that these types of behavior may represent generic (rather than unusual) dynamics as parameters are systematically varied. The extent of phase space in which these behaviors will be observed appear to be very small, but since they do depend on parameters, there may well be circumstances in which the ranges are larger than those found here. Furthermore, since many transitions of heart dynamics happen only once, leading to a person's death, the rare appearance of dynamics over limited regions of parameter space in a mathematical model may still be a worthwhile and practically important direction for analysis.

Acknowledgments. We thank Rod Edwards, Thomas Gedeon, and Eusebius Doedel for helpful conversations and Eric Cytrynbaum for clarification of the Morris–Lecar system under consideration.

REFERENCES

[1] C. Antzelevitch, J. Jalife, and G. K. Moe, *Characteristics of reflection as a mechanism of reentrant arrhythmias and its relationship to parasystole*, Circulation, 61 (1980), pp. 182–191.

[2] O. V. Aslanidi and O. A. Mornev, *Soliton-like regimes and excitation pulse reflection (echo) in homogeneous cardiac purkinje fibers: Results of numerical simulations*, J. Biol. Phys., 25 (1999), pp. 149–164.

[3] D. S. Auerbach, K. R. Grzeda, P. B. Furspan, P. Y. Sato, S. Mironov, and J. Jalife, *Structural heterogeneity promotes triggered activity, reflection and arrhythmogenesis in cardiomyocyte monolayers*, J. Physiol., 589 (2011), pp. 2363–2381.

[4] C. Cabo and R. C. Barr, *Reflection after delayed excitation in a computer model of a single fiber*, Circ. Res., 71 (1992), pp. 260–270.

[5] L. Collatz, *The Numerical Treatment of Differential Equations*, Springer-Verlag, New York, 1966.

[6] H. Croisier, M. R. Guevara, and P. C. Dauby, *Bifurcation analysis of a periodically forced relaxation oscillator: Differential model versus phase-resetting map*, Phys. Rev. E, 79 (2009), 16209.

[7] E. N. Cytrynbaum and T. J. Lewis, *A global bifurcation and the appearance of a one-dimensional spiral wave in excitable media*, SIAM J. Appl. Dyn. Syst., 8 (2009), pp. 348–370.

[8] M. Delmar, D. C. Michaels, T. Johnson, and J. Jalife, *Effects of increasing intercellular resistance on transverse and longitudinal propagation in sheep epicardial muscle*, Circ. Res., 60 (1987), pp. 780–785.

[9] E. J. Doedel and B. E. Oldeman, *AUTO-07P: Continuation and Bifurcation Software for Ordinary Differential Equations*, http://cmvl.cs.concordia.ca/auto/ (2007).

[10] J. R. Dormand and P. J. Prince, *A family of embedded Runge–Kutta formulae*, J. Comput. Appl. Math., 6 (1980), pp. 19–26.

[11] G. B. Ermentrout and J. Rinzel, *Reflected waves in an inhomogeneous excitable medium*, SIAM J. Appl. Math., 56 (1996), pp. 1107–1128.

[12] T. Gedeon and L. Glass, *Continuity of resetting curves for FitzHugh-Nagumo equations on the circle*, Fields Inst. Commun., 21 (1999), pp. 225–236.

[13] L. Glass and M. E. Josephson, *Resetting and annihilation of reentrant abnormally rapid heartbeat*, Phys. Rev. Lett., 75 (1995), pp. 2059–2062.

[14] L. Glass, Y. Nagai, K. Hall, M. Talajic, and S. Nattel, *Predicting the entrainment of reentrant cardiac waves using phase resetting curves*, Phys. Rev. E, 65 (2002), 021908.

[15] L. Glass and A. T. Winfree, *Discontinuities in phase resetting experiments*, Am. J. Physiol. Reg. I, 15 (1984), pp. 251–258.

[16] J. Guckenheimer, *Isochrons and phaseless sets*, J. Math. Biol., 1 (1975), pp. 259–273.

[17] J. Guckenheimer and P. Holmes *Nonlinear Oscillations, Dynamical Systems, and Bifurcation of Vector Fields*, Springer-Verlag, New York, 1983.

[18] M. R. Guevara, A. Shrier, and L. Glass, *Phase resetting of spontaneously beating embryonic ventricular heart cell aggregates*, Am. J. Physiol. Heart C., 251 (1986), pp. 1298–1305.

[19] K. Hall and L. Glass, *How to tell a target from a spiral: The two probe problem*, Phys. Rev. Lett., 82 (1991), pp. 5164–5167.

[20] R. W. Joyner, *Effects of the discrete pattern of electrical coupling on propagation through an electrical syncytium*, Circ. Res., 50 (1982), pp. 192–200.

[21] J. P. Keener, *Propagation and its failure in coupled systems of discrete excitable cells*, SIAM J. Appl. Math., 47 (1987), pp. 556–572.

[22] J. P. Keener, *The effects of discrete gap junction coupling on propagation in myocardium*, J. Theoret. Biol., 148 (1991), pp. 49–82.

[23] N. Kopell and L. N. Howard, *Target patterns and horseshoes from a perturbed central-force problem: Some temporally periodic solutions to reaction-diffusion equations*, Stud. Appl. Math., 64 (1981), pp. 1–56.

[24] B. Krauskopf and H. M. Osinga, *Computing invariant manifolds via the continuation of orbit segments*, in Numerical Continuation Methods for Dynamical Systems, B. Krauskopf, H. M. Osinga, and J. M. Galán-Vioque, eds., Springer-Verlag, New York, 2007.

[25] T. Krogh-Madsen and D. J. Christini, *Resetting and termination of reentry in a loop-and-tail cardiac model*, Phys. Rev. E, 77 (2008), 011916.
[26] T. Krogh-Madsen, L. Glass, E. J. Doedel, and M. R. Guevara, *Apparent discontinuities in the phase-resetting response of cardiac pacemakers*, J. Theoret. Biol., 230 (2004), pp. 499–519.
[27] M. Krupa, B. Sandstede, and P. Szmolyan, *Fast and slow waves in the Fitzhugh-Nagumo equation*, J. Differential Equations, 133 (1997), pp. 49–97.
[28] T. Nomura and L. Glass, *Entrainment and termination of reentrant wave propagation in a periodically stimulated ring of excitable media*, Phys. Rev. E, 53 (1996), pp. 6353–6360.
[29] H. M. Osinga and J. Moehlis, *Continuation-based computation of global isochrons*, SIAM J. Appl. Dyn. Syst., 9 (2010), pp. 1201–1228.
[30] S. Richter and P. Brugada, *Bidirectional ventricular tachycardia*, J. Am. Coll. Cardiol., 54 (2009), 1189.
[31] J. Rinzel and J. B. Keller, *Traveling wave solutions of a nerve conduction equation*, Biophys. J., 13 (1973), pp. 1313–1337.
[32] S. Rohr, J. P. Kucera, V. G. Fast, and A. G. Kléber, *Paradoxical improvement of impulse conduction in cardiac tissue by partial cellular uncoupling*, Science, 275 (1987), pp. 841–844.
[33] Y. Rudy and W. L. Quan, *A model study of the effects of the discrete cellular structure on electrical propagation in cardiac tissue*, Circ. Res., 61 (1987), pp. 815–823.
[34] B. Sandstede and A. Scheel, *Defects in oscillatory media: Toward a classification*, SIAM J. Appl. Dyn. Syst., 3 (2004), pp. 1–68.
[35] B. Sandstede and A. Scheel, *Period-doubling of spiral waves and defects*, SIAM J. Appl. Dyn. Syst., 6 (2007), pp. 494–547.
[36] S. Sinha, K. M. Stein, and D. J. Christini, *Critical role of inhomogeneities in pacing termination of cardiac reentry*, Chaos, 12 (2002), pp. 893–902.
[37] M. S. Spach, W. T. Miller, B. Geselowitz, R. C. Barr, J. M. Kootsey, and E. A. Johnson, *The discontinuous nature of propagation in normal canine cardiac muscle. Evidence for recurrent discontinuities of intracellular resistance that affect the membrane currents*, Circ. Res., 48 (1981), pp. 39–54.
[38] C. F. Starmer, V. N. Biktashev, D. N. Romashko, M. R. Stepanov, O. N. Makarova, and V. I. Krinsky, *Vulnerability in an excitable medium: Analytical and numerical studies of initiating unidirectional propagation*, Biophys. J., 65 (1993), pp. 1775–1787.
[39] A. T. Winfree, *Patterns of phase compromise in biological cycles*, J. Math. Biol., 1 (1974), pp. 73–95.
[40] A. T. Winfree, *The Geometry of Biological Time*, Biomathematics 8, Springer-Verlag, New York, 1980.